



# Optics Letters

## Design of a three-phase amplitude macro-pixel full-color complex spatial light modulator with an in-cell geometric phase retardation layer

SEHWAN NA,<sup>1</sup> SOOBIN KIM,<sup>1</sup> JONGHYUN LEE,<sup>1</sup>  YUNHEE KIM,<sup>2</sup> AND HWI KIM<sup>1,\*</sup> 

<sup>1</sup>Department of Electronics and Information Engineering, Korea University, 2511 Sejong-ro, Sejong 30019, Republic of Korea

<sup>2</sup>Samsung Advanced Institute of Technology (SAIT), Samsung Electronics, Suwon, Gyeonggi-do, Republic of Korea

\*Corresponding author: hwikim@korea.ac.kr

Received 6 September 2022; revised 13 October 2022; accepted 15 October 2022; posted 20 October 2022; published 8 November 2022

**Complex spatial light modulation, which can simultaneously control the amplitude and phase of light, is an essential optical technology for holographic display. We propose a twisted nematic liquid crystal (TNLC) mode with an in-cell type embedded geometric phase (GP) plate for full-color complex spatial light modulation. The proposed architecture provides an achromatic full-color complex light modulation capability in the far-field plane. The feasibility and working characteristics of the design are validated through numerical simulation.** © 2022 Optica Publishing Group

<https://doi.org/10.1364/OL.475087>

Complex spatial light modulators (SLMs), which can simultaneously modulate the amplitude and phase of a light field, are considered essential optical devices in a wide range of optical applications, such as digital holography, optical imaging, and optical computing [1,2]. Since a complex SLM can generate a designed optical wave front without direct current (DC) and conjugate terms, it has been actively researched as a core technology for high-quality three-dimensional (3D) holographic image generation. In practice, because a complex SLM does not require an additional noise filtering system to eliminate DC and conjugate terms, it can realize scaled-down holographic displays, and this advantage is a driving force for its application to recent augmented reality display technology. Recently, we proposed a dual-layer complex SLM architecture for generating holographic 3D images [3]. However, we have found the construction of efficient pixel-to-pixel optical interconnections between distant dual panels to be challenging. Thus, a method of achieving highly tolerable optical interconnections needs to be devised.

For structural simplicity, the single-panel complex SLM structure based on a macro-pixel has been actively researched. A double-phase hologram (DPH) complex SLM that can generate a complex wave field through the interference of the adjacent double pixels of a phase-only SLM with passive polarization-sensitive components in monochromatic color was introduced by Reichelt et al. in Ref. [4]. The adjacent double pixels on the phase-only SLM were designed with a scaled-down complex light modulation architecture. The additional optical functional layers are added to the phase-only SLMs. Thus, alignment issues

still exist, as they do in the dual-layer SLM, so in practice the DPH macro-pixel cannot represent a perfect dark-field.

In-cell technology is a promising approach to resolving the alignment issue in the construction of complex SLMs. This technology embeds optically functional layers inside the liquid crystal (LC) panel, thereby eliminating the possible misalignment factors associated with add-on type structures that stack the optical layers on top of the LC panel. In-cell touch technology, which embeds touch sensor panels inside display panels, has commercialized thinner and lighter advanced displays that are commonly applied to mobile and tablet displays [5]. An in-cell retarder can also generate two images with different polarization states for the left and right eyes in a stereoscopic 3D display [6]. The retarder is embedded inside the LCD panel reducing both misalignment and the gap distance between the pixels and retarder to alleviate the cross talk problem and expand the viewing angle of stereoscopic 3D displays [7,8]. Overall, although various advanced SLMs have been developed, a complex SLM based on in-cell technology for complex wave field generation has not yet been proposed.

In this paper, we propose a single-panel complex SLM based on in-cell technology to completely control the amplitude and phase distribution of the optical field at the far-field plane. The employed in-cell device is a geometric phase (GP) plate, which will be placed inside the amplitude-only SLM panel and perform three-level phase modulation at the primary color R (633 nm), G (532 nm), and B (473 nm) wavelengths. The in-cell GP plate improves pixel-to-pixel alignment and reduces the diffraction effect of light. The complex number decomposition method into three-phase amplitude modulation is adopted. The three-phase amplitude modulation combines three amplitude sub-pixels and controls the amplitude and phase of the light field at the far-field plane by adjusting the amplitude values of each of the sub-pixels in the complex macro-pixel. The linear combination of the three decomposed amplitude components represents a grouped complex valued single pixel as a result of the interference of three-phase light wave components as

$$Ae^{j\phi} = A_1e^{j\phi_1} + A_2e^{j\phi_2} + A_3e^{j\phi_3}, \quad (1)$$

where,  $A_1$ ,  $A_2$ , and  $A_3$  are the amplitude values ranging from 0 to 1, and  $\phi_1$ ,  $\phi_2$ , and  $\phi_3$  are the phase retardations of the three

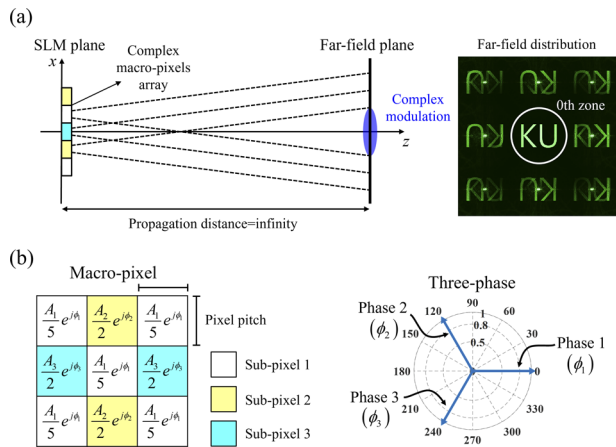


**Fig. 1.** (a) Simulation schematic of the complex SLM in the far-field plane, (b)  $3 \times 3$  macro-pixel unit and three-phase basis of the sub-pixels.

sub-pixels. For high efficiency complex modulation,  $\phi_1$ ,  $\phi_2$ , and  $\phi_3$  should be set to angles with  $120^\circ$  intervals. Note that Eq. (1) means the three-phase basis decomposition of a given complex value in the complex plane [Fig. 1(a)]. Figure 1(a) shows the diffraction image from a complex SLM with a  $3 \times 3$  macro-pixel unit in the far field. This  $3 \times 3$  macro-pixel unit consists of nine pixels with three-phase retardation and variable amplitudes as shown in Fig. 1(b). The calculated complex CGH is represented by a linear combination of the three complex values and encoded in a  $3 \times 3$  macro-pixel for the wavelength of 532 nm. The working principle of the macro-pixel is based on the interference between adjacent sub-pixels in the zeroth diffraction zone of the far-field plane. The diffraction image without the DC and conjugate terms is obtained in the zeroth diffraction zone.

Let us investigate the physical pixel architecture of the full-color three-phase amplitude SLM. Figure 2(a) schematically illustrates the single-pixel architecture of the add-on type complex SLM with a periodic surface relief (SR) three-phase retardation plate on top of an amplitude SLM panel. The SR phase plate is designed to provide phase retardation fit to the  $3 \times 3$  macro-pixel unit. The phase retardation  $\phi$  is determined by the thickness of the phase plate,  $t = \lambda\phi / (2\pi(n - 1))$ , where  $n$  is the refractive index of the material. The refractive index of the period SR phase plate was set to 1.5. The RGB pixel is a sub-pixel, and  $3 \times 3$  nine sub-pixels comprise a single macro-pixel. The SR thickness of the phase plate can be optimized for a single specific operating frequency. Deviation in phase retardation is inevitable when the operating wavelength changes. This monochromatic phase retardation places limitations on RGB full-color operation. The SR phase plate should have at least seven-level SR for RGB wavelengths, but the fabrication and accurate alignment process of a seven-level phase plate and the RGB SLM pixels is cumbersome. When we use a three-level SR phase plate optimized for the green wavelength, a phase deviation in the phase plate for red and blue wavelengths arises. In Fig. 2(b), the three-phase basis and the resultant complex modulation ranges for the RGB wavelengths are compared in the complex plane. The three-phase basis of the central wavelength of 532 nm forms an equilateral triangle with regular phase retardation at  $120^\circ$  intervals, presenting a complete full-circular complex modulation range. This analysis assumes that normal incident optical waves propagate from the bottom polarizer to

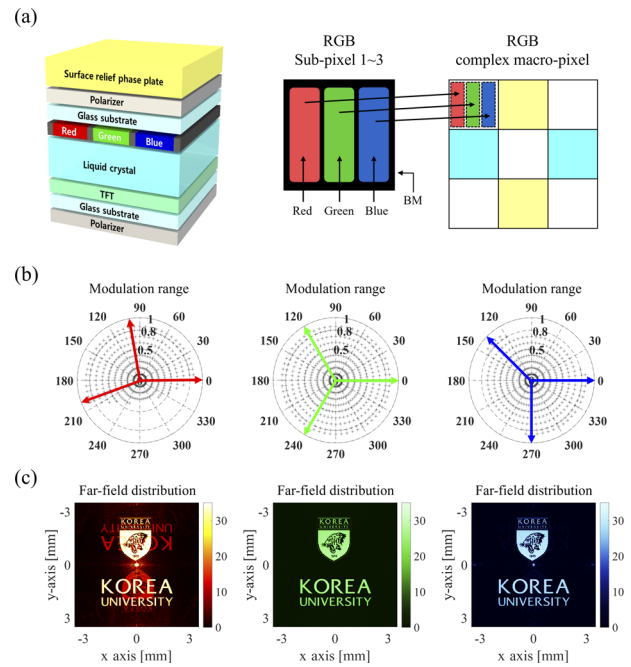


**Fig. 2.** (a) Single-pixel architecture of add-on type complex SLM, (b) three-phase basis and complex modulation range, and (c) diffraction images in the far-field plane.

the SR phase plate. At the 532 nm wavelength, the diffraction image in the zeroth zone of the far-field plane does not accompany DC and conjugate noise components as shown in Fig. 2(c). In contrast, the triangle patterns of the three-phase basis at the wavelengths of 633 nm and 473 nm deviate from the equilateral triangle, leading to a reduction of the complex modulation range, which causes an abrupt degradation in efficiency. In Fig. 2(c), the diffraction images for the red and blue wavelengths are contaminated by the DC or conjugate noise terms. This vulnerability in the phase retardation hinders full-color complex modulation on the single-panel SLM. The issue is that the periodic phase plate is highly wavelength dependent. Furthermore, the add-on type SLM structure also causes inter-pixel cross talk and misalignment between optical elements. Therefore, we need to devise an achromatic phase retardation plate for full-color complex SLMs and to improve inter-layer alignment reliability through an in-cell design.

An in-cell design of a sub-pixel of the full-color complex SLM is presented in Fig. 3(a), which corresponds to a sub-pixel in a  $3 \times 3$  complex macro-pixel. The macro-pixel topology is assumed to be identical to that of the conventional add-on structure shown in Fig. 2(a). The specific design point is that the GP retardation layer is embedded inside the SLM, fabricated between the color filter layer and the upper glass substrate. The twisted nematic liquid crystal (TNLC) mode is employed for sub-pixel amplitude modulation. The optimally designed GP layer has achromatic phase retardation characteristics, unlike the SR phase plate in phase modulation. The design of the in-cell architecture considered the feasibility of the industrial-level manufacturing process.

Before delving into the optimal design of the achromatic GP layer, we demonstrate the overall performance of the proposed architecture in Fig. 3. The complex light modulation range of the optimized SLM architecture at the RGB primary

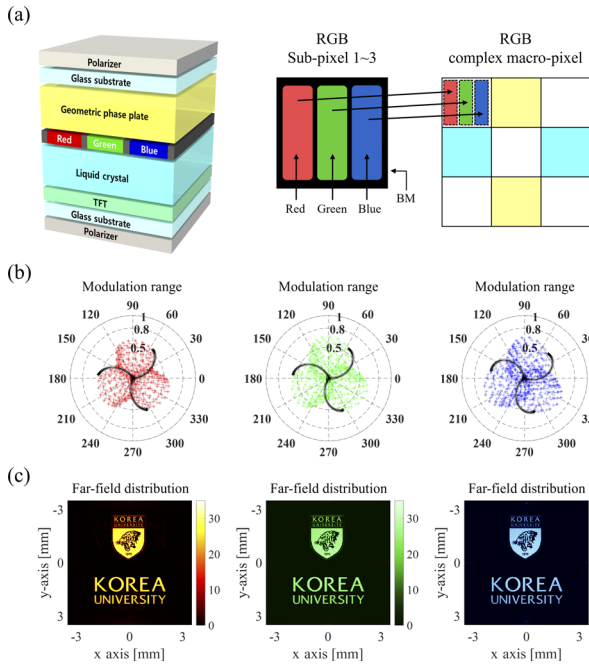


**Fig. 3.** (a) Single-pixel architecture of in-cell type complex SLM, (b) three-phase basis and complex modulation range by three-phase amplitude modulation, and (c) diffraction images in the far-field plane.

wavelengths is numerically analyzed. For design and analysis, an electronic model based on the Fourier modal method (FMM) has been developed [9]. Interestingly, the three-phase basis for the RGB wavelengths is obtained in the form of a twisted pinwheel [Fig. 3(b)]. The proposed architecture achieves full complex modulation with a maximum amplitude of 0.35, which is equivalent to 12.25% complex modulation efficiency. In practice, the complex modulation efficiency is associated with the degree of dependency of amplitude and phase modulation, which is discussed later. The diffraction images in the far-field plane are shown in Fig. 3(c). The obtained diffraction images for the RGB wavelengths show the complex field characteristics with highly reduced DC and conjugate noises. This verifies that the proposed pixel architecture can provide full-color complex light modulation in the zeroth zone of the far-field plane.

To achieve optimal performance, the design of the in-cell structure of the achromatic GP layer and TNLC needs optimization. The GP device modulates the phase of light that passes through the TNLC layer and color filter layer. The GP layer converts right circularly polarized (RCP) light to left circularly polarized (LCP) light with a specific phase retardation. Figure 4(a) shows the LC cell structure of an in-cell GP layer in a part of the in-cell pixel architecture shown in Fig. 3(a). We adopt a four-LC layer multi-twist structure with mirror symmetry as the GP layer template [10,11]. This four-layer LC structure was proven to be highly efficient compared to the two-layer and three-layer structures. Considering the amplitude modulation of the TNLC, we aim to realize an in-cell GP retarder that not only features near 100% efficiency, but also perfectly converts the incident circular polarized light to its cross-polarization counterpart at normal incidence. The first and fourth LC layers have the same cell thickness and twist angles in opposite

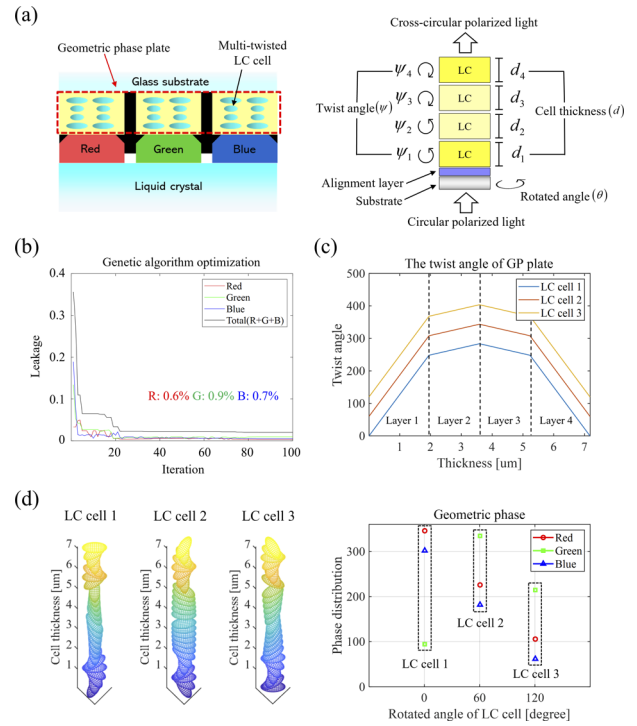


**Fig. 4.** (a) Schematics of GP retardation layer in a part of the in-cell pixel architecture, (b) optimization results for minimizing co-polarization of the transmitted beam, (c) optimized twist angle and cell thickness of LC cells, and (d) phase retardation characteristics of the GP LC cell 1, 2, and 3.

directions. Likewise, the second and third LC layer have the same cell thickness and twist angles in opposite directions. The genetic algorithm was employed to optimize the four independent structural parameters,  $d_1 = d_4$ ,  $d_2 = d_3$ ,  $\psi_1 = -\psi_4$ , and  $\psi_2 = -\psi_3$  for a near 100% efficient RGB in-cell GP layer with a birefringence of  $\Delta n = 0.15$  ( $n_e = 1.65$ ,  $n_o = 1.50$ ). We reduced the co-polarization leakage in transmittance to less than 1% for the LCP (or RCP) incident light wave at the RGB wavelengths [Fig. 4(b)], meaning that the phase retardation efficiency of the cross-polarized component is larger than 99% at the RGB wavelengths.

For a three-phase basis, we need to analyze the GP as the optimized LC cell is rotated. The rotated LC cells should have  $120^\circ$  phase difference to each other. Figure 4(c) shows the numerical results of the optimized twist angle and thickness of LC cells. The LC cells 1, 2, and 3 with rotated angles of  $0^\circ$ ,  $60^\circ$ , and  $120^\circ$ , respectively, generate the three geometric phases  $\phi_1$ ,  $\phi_2$ , and  $\phi_3$ . The genetic algorithm dictates that the total thicknesses of the optimized LC cells are the same at  $7.192 \mu\text{m}$ . The optimized GP layers (LC cells 1, 2, 3) produce  $120^\circ$  phase differences at the RGB wavelengths as shown in Fig. 4(d).

TNLC is twisted in the direction of the optical axis, which adjusts the light intensity by rotating the tilt angle of the LC under electric voltage control. While normal TNLC displays work with crossed linear polarizers, in the proposed in-cell structure, the amplitude modulation of the circularly polarized light must be obtained through the cascaded structure of the TNLC and GP layers. Thus, we need to optimize the TNLC cell thickness to enable the gray-scale amplitude modulation of circularly polarized light waves. When the extraordinary and

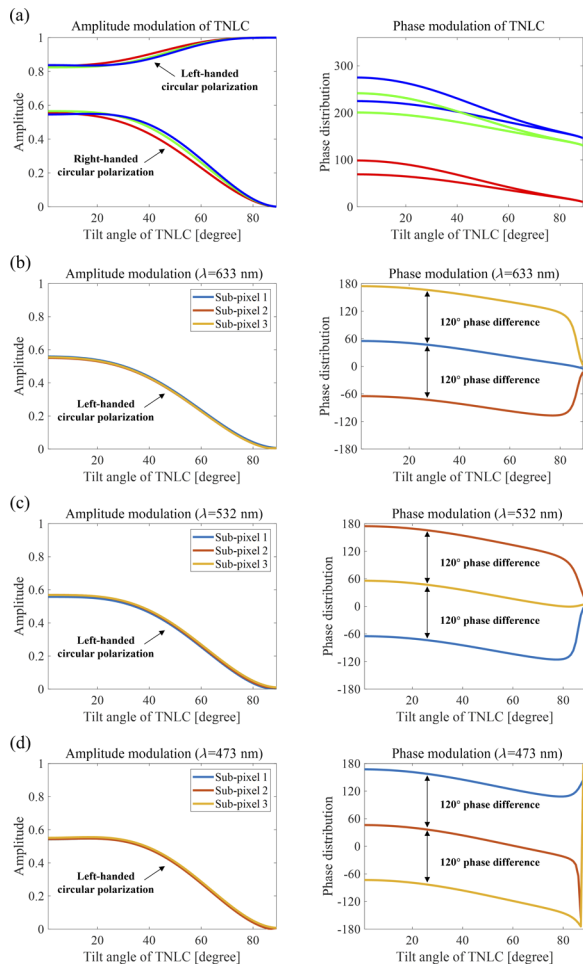


**Fig. 5.** Modulation characteristics of (a) the designed TNLC layer, and (b)–(d) the sub-pixels of the in-cell pixel architecture.

ordinary refractive indices of the TNLC are set to  $n_e = 1.5587$  and  $n_o = 1.4765$ , respectively, the parametric study found the optimal cell gap to be  $3 \mu\text{m}$ . Figure 5(a) shows the amplitude modulation characteristics of the TNLC under a normally incident LCP. The LCP light wave propagating through the TNLC layer is split into RCP components (cross-polarized) and LCP components, and the phase modulation of the TNLC is nearly flat with a slight split according to polarization status and wavelength in Fig. 5(a).

We will mainly exploit the gray-scale modulated RCP component, while the LCP component of the TNLC will be rejected by the top-layer polarizer shown in Fig. 3(a). The bottom and top layers of the pixel architecture are the same LCP polarizer. The primary RCP component is converted to the LCP component through the three-phase GP layer and is continuously transmitted by the top-layer LCP polarizer. In Figs. 5(b)–5(d), the transmitted LCP components of the three sub-pixels under normal LCP incidence work properly in terms of the gray-scale amplitude modulation and the essential  $0$ ,  $120^\circ$ ,  $-120^\circ$  phase modulations with a slight dependency on the amplitude modulation across the entire gray-scale range. This dependency leads to a decrease in the complex modulation efficiency and the twisted pinwheel

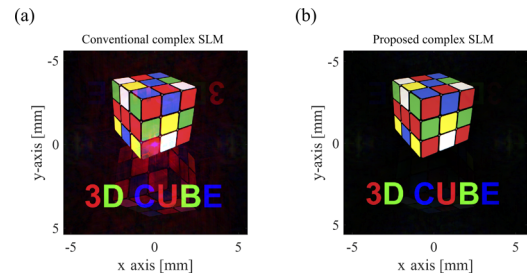


**Fig. 6.** Full-color diffraction images obtained by (a) the add-on type complex SLM, and (b) the in-cell type complex SLM.

pattern shown in the complex modulation range in Fig. 3(b). The proposed architecture presents a maximum 0.35 amplitude modulation in Fig. 1(b), that is equivalent to 12.25%. It is important to note the achievement of a black field. It is also noteworthy that, although the modulation phases of the three-phase GP layer converge to a specific phase at the black field state which corresponds to a near  $90^\circ$  tilt angle at the TNLC layer, the convergence of the phase modulation to a specific value has no effect in the black field representation.

Figure 6 compares the full color diffraction image generated by the conventional add-on type with an SR phase plate with that of the proposed in-cell type in terms of image quality. The result indicates that the in-cell type complex SLM can be used to create ultra-low noise, high-fidelity, full-color, flat-panel holographic displays.

**Funding.** Alchemist Project (MOTIE&KEIT 1415179744, 20019169); Samsung (SRFC-TB1903-05).

**Disclosures.** The authors declare no conflicts of interest.

**Data availability.** Data underlying the results presented in this paper are not publicly available at this time but may be obtained from the authors upon reasonable request.

## REFERENCES

- J. An, K. Won, Y. Kim, J.-Y. Hong, H. Kim, Y. Kim, H. Song, C. Choi, Y. Kim, J. Seo, A. Morozov, H. Park, S. Hong, S. Hwang, K. Kim, and H.-S. Lee, *Nat. Commun.* **11**, 1 (2020).
- J. Park, B. G. Jeong, and S. I. Kim, *et al.*, *Nat. Nanotechnol.* **16**, 69 (2021).
- S. W. Jang, W. Choi, S. Kim, J. Lee, S. Na, S. Ham, J. Park, H. Kang, B. K. Ju, and H. Kim, *Sci. Rep.* **12**, 1 (2022).
- S. Reichelt, R. Häussler, G. Fütterer, N. Leister, H. Kato, N. Usukura, and Y. Kanbayashi, *Opt. Lett.* **37**, 1955 (2012).
- G. Walker and M. Fihn, *Inf. Disp.* **26**, 8 (2010).
- Y. J. Wu, Y. S. Jeng, P. C. Yeh, C. J. Hu, and W. M. Huang, *SID Symposium Digest.* **39**, 260 (2008).
- C.-T. Lee and H. Y. Lin, *Opt. Express* **20**, 1700 (2012).
- K.-S. Bae, U. Cha, Y.-K. Moon, J. W. Heo, Y.-J. Lee, J.-H. Kim, and C.-J. Yu, *Opt. Express* **20**, 6927 (2012).
- H. Kim, J. Park, and B. Lee, *Fourier Modal Method and Its Applications in Computational Nanophotonics* (CRC, 2012).
- W. Chen, Y. Yu, Q. Mu, J. Campos, Q. Wang, S. Li, S. Zhang, and L. Xuan, *Appl. Phys. Lett.* **119**, 101103 (2021).
- R. K. Komanduri, K. F. Lawler, and M. J. Escuti, *Opt. Express* **21**, 404 (2013).